

Transport of magnetically sensitive atoms in a magnetic environment

D.A. Kumpilov^{1,2}, I.A. Pyrkh^{1,2}, I.S. Cojocaru^{1,3,4}, P.V. Trofimova¹, V.A. Khlebnikov¹, P.A. Aksentsev^{1,4}, A.E. Rudnev^{1,2}, A.M. Ibrahimov^{1,2}, O.I. Blokhin^{1,2}, K.O. Frolov^{1,2}, S.A. Kuzmin^{1,2}, D.V. Gaifutdinov^{1,2}, A.K. Zykova¹, D.A. Pershin^{1,3}, V.V. Tsyganok¹, A.V. Akimov^{1,3}

¹*Russian Quantum Center, Bolshoy Boulevard 30, building 1, Skolkovo, 143025, Russia*

²*Moscow Institute of Physics and Technology, Institutskii pereulok 9, Dolgoprudny, Moscow Region 141701, Russia*

³*PN Lebedev Institute RAS, Leninsky Prospekt 53, Moscow, 119991, Russia*

⁴*Bauman Moscow State Technical University, 2-nd Baumanskaya, 5, Moscow, 105005, Russia*

email: a.akimov@rqc.ru

Among interesting applications of cold atoms, quantum simulations attract a lot of attention. In this context, rare-earth ultracold atoms are particularly appealing for such simulators due to their numerous Fano-Feshbach resonances and magnetic dipole moments in the ground state. Creating a quantum gas microscope requires a large optical access that may be achieved using transport of atoms between separate vacuum volumes. We demonstrate that in case of the transport of magnetic atoms the magnetic field can be directly measured and adjusted to reduce additional losses after the transport therefore increasing the efficiency of subsequent evaporation cooling. This approach allows to transfer over 85% of the atoms from the main chamber to the scientific chamber, located 38 cm away with moderate laser power of 26 W without atomic polarization decay

I. INTRODUCTION

Rare-earth ultracold atoms are emerging as an intriguing platform for quantum simulations [1–8]. The presence of f -electrons causes a large magnetic moment in the ground state facilitating long-range interactions [9,10], and a dense spectrum of low-field Feshbach resonances,

providing detailed control over short-range interactions [11–15]. Moreover, rare-earth elements allowed to observe quantum droplets [16–19]. Along with cavity-mediated interactions [20] and spin-orbit coupled quantum gases [21], dipolar gases play a noticeable role in the research of supersolids [22–24]. The quantum gas microscope has been recently demonstrated with Erbium atoms [25].

A quantum gas microscope with ultracold atoms requires a high numerical aperture. Although it can be achieved in a single-chamber experiment design [25,26], creation of separate vacuum volumes is more common [27–33]. A number of methods to transfer atoms between two vacuum chambers have been developed. One can use magnetic fields to transport atoms captured in magneto-optical traps (MOTs) [34,35]. Also, shifting the focus of the optical dipole trap (ODT) beam using translation stages [36], focus-tunable lenses [37,38] and 1D optical lattices [39] allows to move atomic clouds. By transporting atoms in the ODT to the volume of the glass cell, a quantum microscope with non-magnetic ytterbium atoms was achieved [40].

Contrarily, when the atoms have large magnetic moment, their transport becomes more complicated due to a number of reasons. First, the presence of an external magnetic field gradient causes an extra force, which affects the motion of the atoms. Next, the high density of Fano-Feshbach resonances typical of rare-earth atoms can cause losses of atoms when the magnetic field changes along the transport trajectory [11,12,15,41]. Finally, non-adiabatic changes in the magnetic field can cause depolarization of an atomic ensemble and subsequent spin-relaxation losses. Although some works reported the optical transport of magnetic atoms with high efficiency, there is no information about these obstacles [13,42]. Perhaps, there were no extra losses during transport because of high power of the ODT beam suppressing the magnetic field forces. Additionally, the depolarization was not indicated possibly because the number of remaining atoms after the spin-relaxation losses was sufficient.

This paper presents a method for reasonably fast optical transport of magnetic dipolar thulium ^{169}Tm atoms. This method exploits the maintenance of the magnetic field during the transport to preserve the polarization of the atoms at the lowest magnetic sublevel $|F = 4, m_F = -4\rangle$ in the ground state $4f^{13}({}^2F^0)6s^2$ with corresponding total electronic momentum $J = \frac{7}{2}$ and nuclear spin $I = \frac{1}{2}$. Moreover, sophisticated tailoring of the focus-tunable waist position compensated for the force from the gradient of the magnetic field. This approach allows to avoid additional

losses during the transport using less power in the ODT beam. Moreover, the approach reduces the spin-relaxation losses after transport that can be very useful for more efficient evaporative cooling and production of quantum degenerate states in the separate vacuum volume.

II. EXPERIMENTAL SETUP

The precooling and trapping stages of the experiment closely followed procedures presented in previous studies [43–48]. The pre-cooling of the atoms was realized via the Zeeman slower and 2D optical molasses operated at the strong transition $4f^{13}({}^2F^o)6s^2 \rightarrow 4f^{12}({}^3H_5)5d_{3/2}6s^2$ with a wavelength of 410.6 nm and a natural width of $\Gamma = 2\pi\gamma = 2\pi \cdot 10.5\text{MHz}$. Following the precooling stage, atoms were loaded into the MOT operating at the weaker transition $4f^{13}({}^2F^o)6s^2 \rightarrow 4f^{12}({}^3H_6)5d_{5/2}6s^2$ with a wavelength of 530.7 nm and a natural width of $\Gamma = 2\pi\gamma = 2\pi \cdot 345.5\text{kHz}$. Then the reduction of MOT light intensity provided the polarization of atoms at the lowest magnetic sublevel $|F = 4; m_F = -4\rangle$ of the ground state [49–53]. The atoms were cooled down to $22.5 \pm 2.5 \mu\text{K}$ and then loaded into the ODT formed by a linearly polarized laser beam waist with a wavelength of 1064 nm.

The MOT was formed in the Kimball Physics MCF800-ExtOct-G2C8A16 UHV vacuum chamber, the scientific chamber was the glass cell. The distance between the centers of the two chambers was measured at 38 cm. To implement the optical transport, the beam waist with the total power of 26 W was created by a system of a focus-tunable lens and a bi-convex lens with focal length $F = 250$ mm (Figure 1a). Variations of the optical power $1/f$ of the focus-tunable lens made it possible to alter the ODT beam waist position by more than 40 cm (Figure 1b) exceeding the distance between the main chamber and the science chamber. The camera mounted on a moving table outside vacuum chamber allowed to measure the beam waist in all the positions and to make it constant experimentally varying δ . The $37 \mu\text{m}$ value of the waist corresponds to the trap depth $430 \mu\text{K}$.

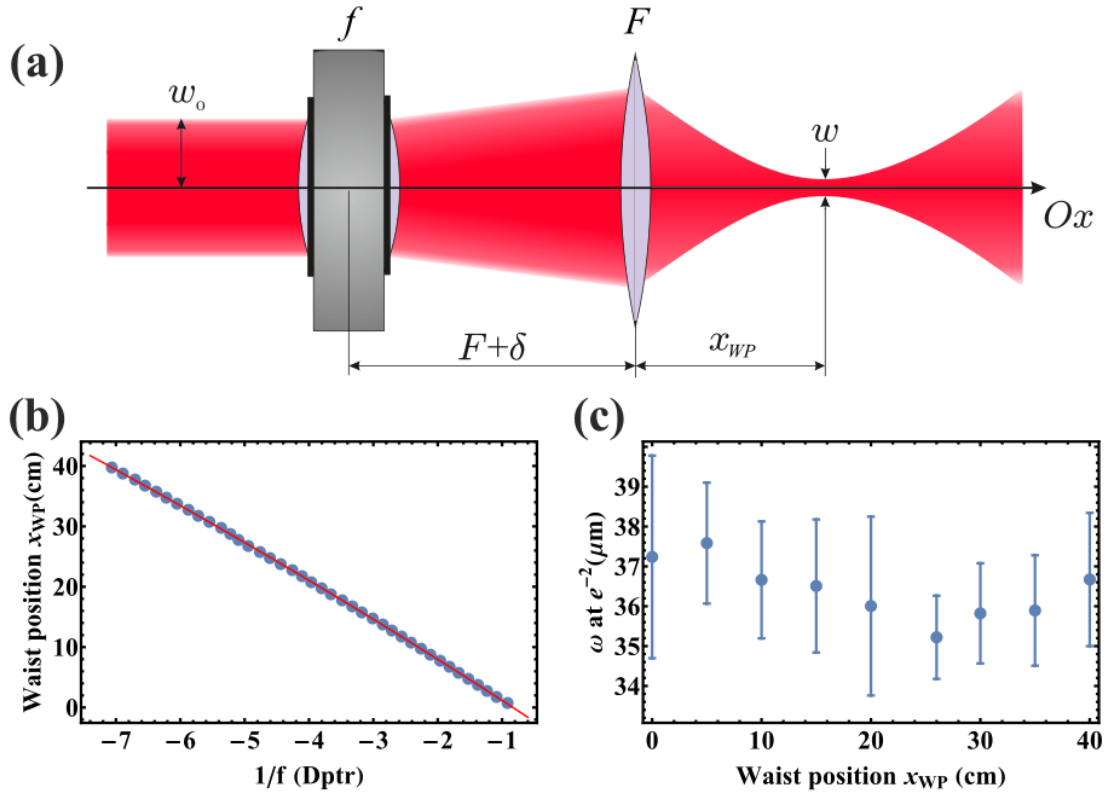


Figure 1. a) Optical scheme of the transport ODT. Initial beam waist w_0 is equal to 2.08 mm. Varying $1/f$ of the tunable lens allowed to move the position of the waist $x_{WP}(t)$. Experimentally varying δ allowed to make the waist value equal to $37 \mu\text{m}$ in all the waist coordinates. b) Waist coordinate relative to the starting point of the transport versus the optical power of the tunable lens. The solid line is a fit of the experimental data with the result of gaussian beam calculations. The error bars are smaller than the point sizes and are not shown. c) The waist of the ODT versus the waist coordinate.

III. MAGNETIC FIELD MEASUREMENT

Shifting the focus of the ODT beam forces the atoms to move along the beam axis. However, all the issues listed in the introduction additionally demand maintaining the magnetic field during the motion. There are at least two limitations on the magnetic field value. On the one hand, previous results revealed a remarkable depolarization in a low magnetic field [54]. To obtain a threshold magnetic field sufficiently suppressing the depolarization, the average polarization m_F was calculated via the Boltzmann formula:

$$\langle m_F \rangle = \frac{1}{Z(B)} \sum_{m_F=-4}^{m_F=4} m_F \text{Exp} \left[-\frac{m_F \mu_B g B}{k_B T} \right], \quad Z(B) = \sum_{m_F=-4}^{m_F=4} \text{Exp} \left[-\frac{m_F \mu_B g B}{k_B T} \right], \quad (1)$$

where B is the magnetic field absolute value, T is the temperature of the atomic cloud, and g is the Lande factor. For $T < 50 \mu\text{K}$ and $m_F < -3.95$, the value of B should exceed 2.27 G (Figure 2). On the other hand, the presence of Feshbach resonances imposes another restriction on the value of the magnetic field. Knowing the resonances spectrum for corresponding temperatures from work [11] and taking into account depolarization, the authors decided to maintain the magnetic field in the region of 3.65–3.95 G free of resonances.

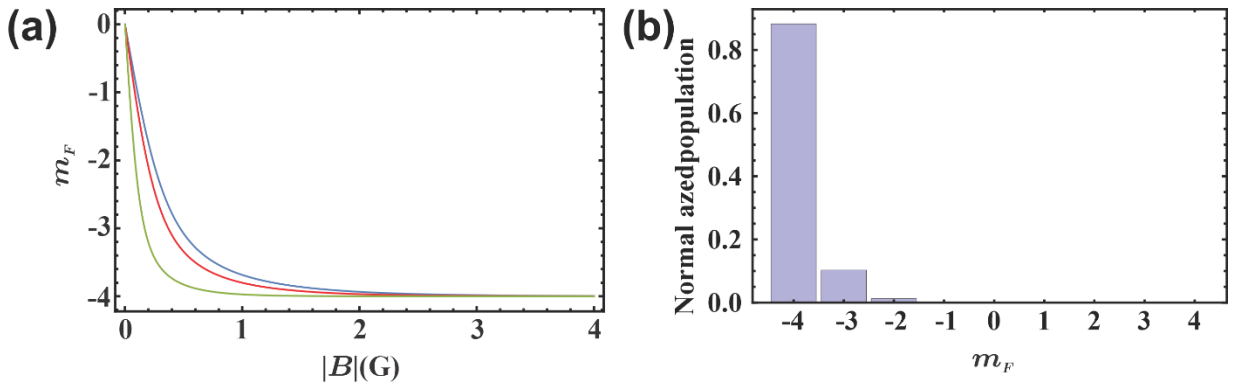


Figure 2. a) Average polarization of the cloud versus holding magnetic field for the green line 20 μK , red line 40 μK , and blue line 50 μK . b) Normalized population of each m_F at holding a magnetic field of 1.2 G with a temperature of 40 μK .

The value of the magnetic field may be maintained by coils, the current of which is synchronized with the shifting the ODT waist. Such an approach requires the knowledge of the magnetic field along the transport trajectory depending on the current in the coils. To measure the magnetic field, the following procedure was performed. The atoms, initially located in the ODT in the main chamber, were transferred to the point x_{WP} , where a 200-ms pulse of 530.7 nm resonance laser radiation illuminated the atoms and then they were returned to the main vacuum chamber where the absorption imaging on 410.6 nm transition was performed (see Figure 3a). During the resonance pulse the magnetic field was created by the current in the MC coils. The frequency of the 530.7 nm laser beam was scanned using an acousto-optic modulator (AOM) around the transition frequency. Scanning the frequency of elliptically polarized green light along with subsequent imaging provides the resonance picture where one can determine two transitions $|F = 4, m_F = -4\rangle \rightarrow |F = 5, m_F = -4\rangle$ (π -transition) and

$|F = 4, m_F = -4\rangle \rightarrow |F = 5, m_F = -3\rangle$ (σ^+ -transition) (see Figure 3c). The spacing between the two resonances is determined by the absolute value of the magnetic field B in the region near x_{WP} according to the relation

$$\nu(|4, -4\rangle \rightarrow |5, -3\rangle) - \nu(|4, -4\rangle \rightarrow |5, -4\rangle) = \frac{\mu_B g_5}{h} B, (2)$$

where $\nu(|4, -4\rangle \rightarrow |5, -3\rangle)$ is the frequency of σ^+ -transition, $\nu(|4, -4\rangle \rightarrow |5, -4\rangle)$ – the frequency of π -transition, μ_B – the Bohr magneton, h – the Planck constant, $g_5 = 1.008$ – the Lande factor for $F = 5$ level. Figure 3b presents the magnetic field as a function of the current in the MC coils and the ODT waist position. For every x_{WP} the interpolating function is $\sqrt{(kI)^2 + B_0^2}$.

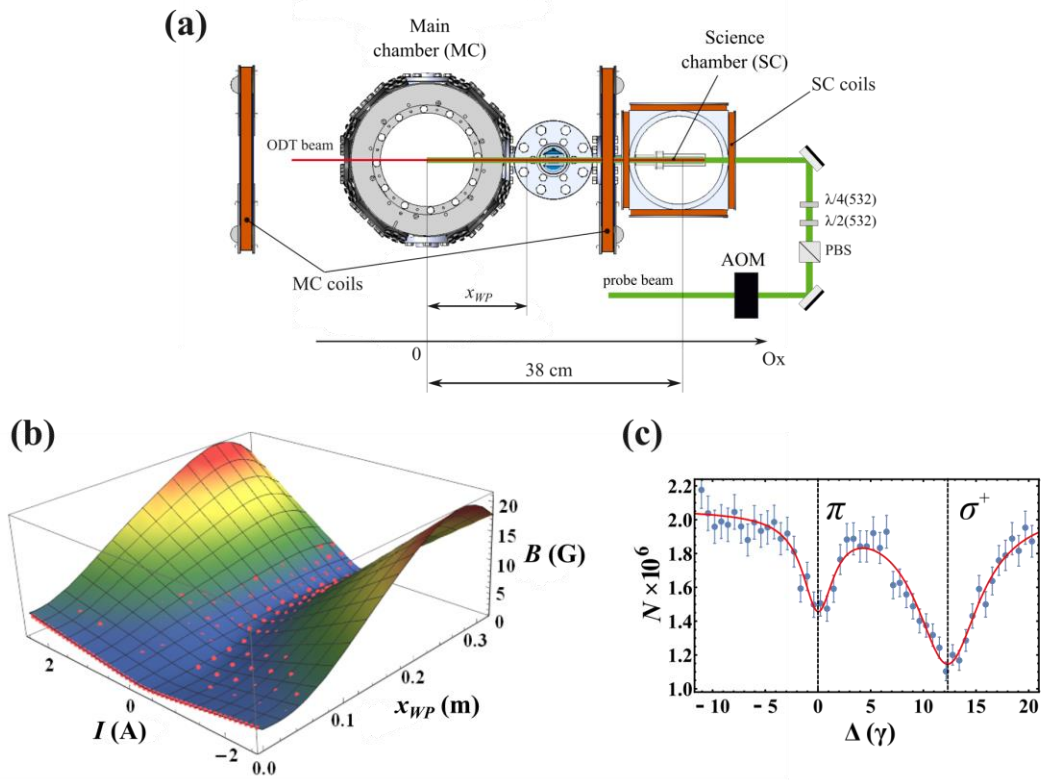


Figure 3. a) Setup of the magnetic field calibration experiment with optical resonance. The Main chamber (MC) coils were used to adjust the magnetic field along the transport trajectory. The science chamber (SC) coils were not used for the transport. The AOM was used to tune the frequency of the probe beam to obtain the graphs similar to the one in (c). b) Absolute value of the magnetic field as a function of the current in the MC coils and the ODT waist position interpolated by

the experimentally obtained points. c) Typical optical resonances in the magnetic field calibration experiment. The plot is given in the number of atoms N vs detuning from atomic resonance Δ in units of γ . Solid line is fit of experimental data with sum of two Lorentzian functions.

IV. OPTICAL TRANSPORT

To perform the optical transport, the focus of the ODT beam is moved and the atoms are forced to follow the dipole force potential minimum. Given the dynamics of the position of the waist $x_{WP}(t)$, the dipole force along the Ox axis exerted on an atom with the coordinate x is determined by the potential

$$U(x, x_{WP}(t)) = - \frac{2\alpha P}{\pi (w_0(x_{WP}(t)))^2 \left(1 + \left(\frac{x_{WP}(t) - x}{x_{REL}} \right)^2 \right)}. \quad (3)$$

Here $w_0(x_{WP}(t))$ is the ODT beam waist depending on its position $x_{WP}(t)$, α – the polarizability of the thulium atom in the ODT, P – the total power of the ODT beam, x_{REL} – the Rayleigh length of the ODT beam. Experimentally, the $x_{WP}(t)$ is set via a focus-tunable lens using a preliminary measured calibration (Figure 1c).

Previously obtained calibration (see Figure 3b) allowed to adjust the spatial profile of the magnetic field along the transport trajectory via the sequence of current in the MC coils $I(t)$. The magnetic field exerts a force on magnetic atoms depending on the gradient

$$\vec{F}_m = \nabla(\vec{\mu}\vec{B}) = \nabla\left(\mu \frac{\vec{B}}{B}\vec{B}\right) = \mu\nabla B, \quad (4)$$

where $\mu = m_F \mu_B g_5$ is the magnetic dipole moment of the atom. Note that the force depends only on the gradient of the magnetic field value because the magnetic moments of the atoms are aligned with the field. Consequently, the motion of the center of mass of a cloud of atoms along the Ox axis governed by Newton's second law was considered:

$$m\ddot{x}_{CM}(t) = F_{mx}(x_{CM}(t)) - \nabla U(x, x_{WP}(t)) \Big|_{x=x_{CM}(t)}, \quad (5)$$

where $x_{CM}(t)$ – the position of the center of mass of a cloud of atoms along the Ox axis. According to the consideration in the section III, the magnetic field was set to $B_0 = 3.8G$ at every point of $x_{CM}(t)$.

The total duration of the transport has several restrictions. A bound from below is set by the characteristic time $T_0 = \nu_x^{-1}$, where ν_x is an ODT frequency along the transport axis: a very fast ramp with time $T \ll T_0$ would be simply ignored by atoms and they would just leave the trap. A bound from above is set by the lifetime of atoms in the ODT measured not to exceed 9 s. Moreover, transferred atoms can oscillate after x_{WP} reaches the final value and stops in time.

The center of mass of a cloud of atoms was set up to move the distance l and duration T with an acceleration changing by $\sin^2(t)$ function [37]. Modeling results and test experiments led to the selection of $T = 20T_0$ to diminish the final oscillations of the atomic cloud. Practically, the final result weakly depended from the frequency factor in the range from 16 to 22. By solving equation (5), one can find the needed profile $x_{WP}(t)$ (see Figure 4b). With this profile, the optical force would indeed compensate for the magnetic force during the entire transport (see Figure 4c). The desired trajectory $x_{CM}(t)$ and acceleration of a center of mass are presented in Figure 4d.

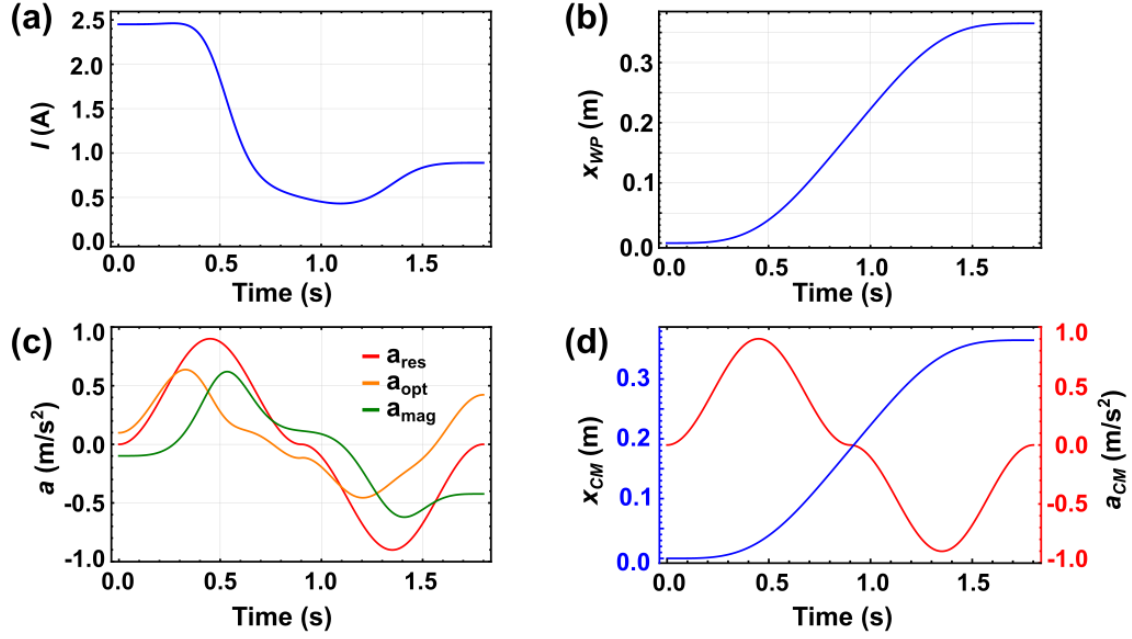


Figure 4. a) Optimal function of current in magnetic coils during optical transport obtained from solving equation (5). The amplitude of the magnetic field in the CM position is constant. b) Resulting optimal optical power versus time. c) Acceleration of CM versus time (red line) and accelerations of CM from magnetic force (green line) and optical dipole force (blue line) d) Model of CM motion. The blue line is a coordinate of CM of the cloud versus time, red line is an acceleration of CM of the cloud versus time.

The obtained $x_{WP}(t)$ function made it possible to move more than $5.4 \cdot 10^6$ atoms to a distance of 38 cm. The efficiency of the transport constituted the value of 0.85 compared to the number of atoms in the ODT measured in the main chamber without transporting them (Figure 5). The decay graph of atoms transferred without maintaining the magnetic field reveals the losses stronger than ones from background collisions. On the contrary, the decay of atoms after the transport with the magnetic field maintaining reveals only the losses from the background collisions. Given the fact that the temperature in both cases was measured to be approximately the same, the maintaining of the magnetic field significantly increases the initial phase space density for the evaporative cooling. Also, one can try to further improve the efficiency of transport with the machine learning approach [11,55].

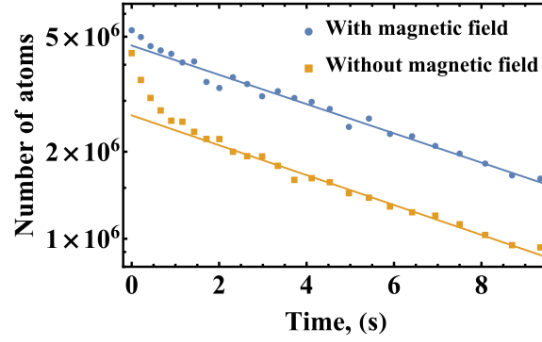


Figure 5. The decay rates of atomic cloud transferred with (blue dots) and without (orange dots) maintaining the magnetic field during transport.

V. CONCLUSION

In summary, the optical transport of magnetic thulium atoms was implemented. The measurement of the magnetic field along the transport made it possible to maintain it constant to reduce the losses related to the Fano-Feshbach resonance spectrum and to maintain the $|F = 4, m_F = -4\rangle$ state of atoms. The force of the magnetic field gradient was compensated for by a sophisticated ramp for the lens with a tunable focus. As a result, $5.4 \cdot 10^6$ atoms were transported to a distance of 38 cm compared to $6.4 \cdot 10^6$ atoms remaining in the ODT without transport after the same period of storage time, as the time used for storage.

VI. ACKNOWLEDGMENTS

This work was supported by Rosatom in the framework of the Roadmap for Quantum computing (Contract No. 868-1.3-15/15-2021 dated October 5, 2021).

VII. REFERENCES

- [1] I. M. Georgescu, S. Ashhab, and F. Nori, Quantum simulation, *Rev Mod Phys* **86**, 153 (2014).
- [2] A. Trautmann, P. Ilzhöfer, G. Durastante, C. Politi, M. Sohmen, M. J. Mark, and F. Ferlaino, Dipolar Quantum Mixtures of Erbium and Dysprosium Atoms, *Phys Rev Lett* **121**, 213601 (2018).
- [3] M. Lu, N. Q. Burdick, and B. L. Lev, Quantum Degenerate Dipolar Fermi Gas, *Phys Rev Lett* **108**, 215301 (2012).

- [4] T. Lahaye, C. Menotti, L. Santos, M. Lewenstein, and T. Pfau, The physics of dipolar bosonic quantum gases, *Reports on Progress in Physics* **72**, 71 (2009).
- [5] S. Baier, D. Petter, J. H. Becher, A. Patscheider, G. Natale, L. Chomaz, M. J. Mark, and F. Ferlaino, Realization of a Strongly Interacting Fermi Gas of Dipolar Atoms, *Phys Rev Lett* **121**, 093602 (2018).
- [6] M. Lu, S. H. Youn, and B. L. Lev, Trapping ultracold dysprosium: A highly magnetic gas for dipolar physics, *Phys Rev Lett* **104**, 063001 (2010).
- [7] A. Petrov, E. Tiesinga, and S. Kotochigova, Anisotropy-induced Feshbach resonances in a quantum dipolar gas of highly magnetic atoms, *Phys Rev Lett* **109**, 103002 (2012).
- [8] G. Natale, T. Bland, S. Gschwendtner, L. Lafforgue, D. S. Grün, A. Patscheider, M. J. Mark, and F. Ferlaino, Bloch oscillations and matter-wave localization of a dipolar quantum gas in a one-dimensional lattice, *Communications Physics* 2022 5:1 **5**, 1 (2022).
- [9] A. J. Olson, D. L. Whitenack, and Y. P. Chen, Effects of magnetic dipole-dipole interactions in atomic Bose-Einstein condensates with tunable s-wave interactions, *Phys Rev A (Coll Park)* **88**, 043609 (2013).
- [10] J. Stuhler, A. Griesmaier, T. Koch, M. Fattori, T. Pfau, S. Giovanazzi, P. Pedri, and L. Santos, Observation of Dipole-Dipole Interaction in a Degenerate Quantum Gas, *Phys Rev Lett* **95**, 150406 (2005).
- [11] V. A. Khlebnikov, D. A. Pershin, V. V. Tsyganok, E. T. Davletov, I. S. Cojocaru, E. S. Fedorova, A. A. Buchachenko, and A. V. Akimov, Random to Chaotic Statistic Transformation in Low-Field Fano-Feshbach Resonances of Cold Thulium Atoms, *Phys Rev Lett* **123**, 213402 (2019).
- [12] V. A. Khlebnikov, V. V. Tsyganok, D. A. Pershin, E. T. Davletov, E. Kuznetsova, and A. V. Akimov, Characterizing the temperature dependence of Fano-Feshbach resonances of ultracold polarized thulium, *Phys Rev A (Coll Park)* **103**, 023306 (2021).
- [13] T. Maier et al., Emergence of Chaotic Scattering in Ultracold Er and Dy, *Phys Rev X* **5**, 041029 (2015).
- [14] A. Frisch et al., Ultracold Dipolar Molecules Composed of Strongly Magnetic Atoms, *Phys Rev Lett* **115**, 203201 (2015).

- [15] K. Baumann, N. Q. Burdick, M. Lu, and B. L. Lev, Observation of low-field Fano-Feshbach resonances in ultracold gases of dysprosium, *Phys Rev A (Coll Park)* **89**, 020701 (2014).
- [16] I. Ferrier-Barbut, H. Kadau, M. Schmitt, M. Wenzel, and T. Pfau, Observation of Quantum Droplets in a Strongly Dipolar Bose Gas, *Phys Rev Lett* **116**, (2016).
- [17] H. Kadau, M. Schmitt, M. Wenzel, C. Wink, T. Maier, I. Ferrier-Barbut, and T. Pfau, Observing the Rosensweig instability of a quantum ferrofluid, *Nature* 2016 530:7589 **530**, 194 (2016).
- [18] L. Chomaz, S. Baier, D. Petter, M. J. Mark, F. Wächtler, L. Santos, and F. Ferlaino, Quantum-Fluctuation-driven crossover from a dilute bose-einstein condensate to a macrodroplet in a dipolar quantum fluid, *Phys Rev X* **6**, (2016).
- [19] M. Schmitt, M. Wenzel, F. Böttcher, I. Ferrier-Barbut, and T. Pfau, Self-bound droplets of a dilute magnetic quantum liquid, *Nature* 2016 539:7628 **539**, 259 (2016).
- [20] J. Léonard, A. Morales, P. Zupancic, T. Esslinger, and T. Donner, Supersolid formation in a quantum gas breaking a continuous translational symmetry, *Nature* 2017 543:7643 **543**, 87 (2017).
- [21] J. R. Li, J. Lee, W. Huang, S. Burchesky, B. Shteynas, F. Ç. Topi, A. O. Jamison, and W. Ketterle, A stripe phase with supersolid properties in spin-orbit-coupled Bose-Einstein condensates, *Nature* 2017 543:7643 **543**, 91 (2017).
- [22] L. Tanzi, E. Lucioni, F. Famà, J. Catani, A. Fioretti, C. Gabbanini, R. N. Bisset, L. Santos, and G. Modugno, Observation of a Dipolar Quantum Gas with Metastable Supersolid Properties, *Phys Rev Lett* **122**, 130405 (2019).
- [23] L. Chomaz et al., Long-Lived and Transient Supersolid Behaviors in Dipolar Quantum Gases, *Phys Rev X* **9**, 021012 (2019).
- [24] M. Guo, F. Böttcher, J. Hertkorn, J. N. Schmidt, M. Wenzel, H. P. Büchler, T. Langen, and T. Pfau, The low-energy Goldstone mode in a trapped dipolar supersolid, *Nature* **574**, 386 (2019).
- [25] L. Su et al., Dipolar quantum solids emerging in a Hubbard quantum simulator, *Nature* 2023 622:7984 **622**, 724 (2023).

- [26] S. Jin, J. Gao, K. Chandrashekhara, C. Götzhäuser, J. Schöner, and L. Chomaz, Two-dimensional magneto-optical trap of dysprosium atoms as a compact source for efficient loading of a narrow-line three-dimensional magneto-optical trap, *Phys Rev A (Coll Park)* **108**, (2023).
- [27] W. S. Bakr, J. I. Gillen, A. Peng, S. Fölling, and M. Greiner, A quantum gas microscope for detecting single atoms in a Hubbard-regime optical lattice, *Nature* **462**, 74 (2009).
- [28] L. W. Cheuk, M. A. Nichols, M. Okan, T. Gersdorf, V. v. Ramasesh, W. S. Bakr, T. Lompe, and M. W. Zwierlein, Quantum-Gas Microscope for Fermionic Atoms, *Phys Rev Lett* **114**, 193001 (2015).
- [29] S. Kuhr, Quantum-gas microscopes: A new tool for cold-atom quantum simulators, *Natl Sci Rev* **3**, 170 (2016).
- [30] E. Haller, J. Hudson, A. Kelly, D. A. Cotta, B. Peaudecerf, G. D. Bruce, and S. Kuhr, Single-atom imaging of fermions in a quantum-gas microscope, *Nat Phys* **11**, 738 (2015).
- [31] R. Yamamoto, J. Kobayashi, T. Kuno, K. Kato, and Y. Takahashi, An ytterbium quantum gas microscope with narrow-line laser cooling, *New J Phys* **18**, 023016 (2016).
- [32] R. Yamamoto, J. Kobayashi, K. Kato, T. Kuno, Y. Sakura, and Y. Takahashi, Site-resolved imaging of single atoms with a Faraday quantum gas microscope, *Phys Rev A (Coll Park)* **96**, 033610 (2017).
- [33] A. Browaeys and T. Lahaye, Many-body physics with individually controlled Rydberg atoms, *Nature Physics* 2020 16:2 **16**, 132 (2020).
- [34] H. J. Lewandowski, D. M. Harber, D. L. Whitaker, and E. A. Cornell, Observation of Anomalous Spin-State Segregation in a Trapped Ultracold Vapor, *Phys Rev Lett* **88**, 070403 (2002).
- [35] M. Greiner, I. Bloch, T. W. Hänsch, and T. Esslinger, Magnetic transport of trapped cold atoms over a large distance, *Phys Rev A (Coll Park)* **63**, 031401 (2001).
- [36] T. L. Gustavson, A. P. Chikkatur, A. E. Leanhardt, A. Görlitz, S. Gupta, D. E. Pritchard, and W. Ketterle, Transport of Bose-Einstein Condensates with Optical Tweezers, *Phys Rev Lett* **88**, 020401 (2001).

- [37] A. Couvert, T. Kawalec, G. Reinaudi, and D. Guéry-Odelin, Optimal transport of ultracold atoms in the non-adiabatic regime, *EPL (Europhysics Letters)* **83**, 13001 (2008).
- [38] J. Léonard, M. Lee, A. Morales, T. M. Karg, T. Esslinger, and T. Donner, Optical transport and manipulation of an ultracold atomic cloud using focus-tunable lenses, *New J Phys* **16**, 093028 (2014).
- [39] S. Schmid, G. Thalhammer, K. Winkler, F. Lang, and J. H. Denschlag, Long distance transport of ultracold atoms using a 1D optical lattice, *New J Phys* **8**, 159 (2006).
- [40] M. Miranda, R. Inoue, Y. Okuyama, A. Nakamoto, and M. Kozuma, Site-resolved imaging of ytterbium atoms in a two-dimensional optical lattice, *Phys Rev A (Coll Park)* **91**, 063414 (2015).
- [41] A. Frisch, M. Mark, K. Aikawa, F. Ferlaino, J. L. Bohn, C. Makrides, A. Petrov, and S. Kotochigova, Quantum chaos in ultracold collisions of gas-phase erbium atoms, *Nature* **507**, 475 (2014).
- [42] T. Pfau, T. Maier, A. Griesmaier, H. Kadau, and M. Schmitt, Narrow-line magneto-optical trap for dysprosium atoms, *Optics Letters*, Vol. 39, Issue 11, Pp. 3138-3141 **39**, 3138 (2014).
- [43] V. V Tsyganok et al., Polarized cold cloud of thulium atom, *Journal of Physics B: Atomic, Molecular and Optical Physics* **51**, 165001 (2018).
- [44] D. A. Pershin, V. V. Tsyganok, V. V. Yaroshenko, V. A. Khlebnikov, E. T. Davletov, E. L. Svechnikov, V. N. Sorokin, P. V. Kapitanova, and A. V. V. Akimov, Microwave Spectroscopy of Ultracold Thulium Atoms, *Bulletin of the Lebedev Physics Institute* **45**, 377 (2018).
- [45] V. V. V Tsyganok, D. A. A. Pershin, E. T. T. Davletov, V. A. A. Khlebnikov, and A. V. V Akimov, Scalar, tensor, and vector polarizability of Tm atoms in a 532-nm dipole trap, *Phys Rev A (Coll Park)* **100**, 042502 (2019).
- [46] V. V. Tsyganok et al., Losses of thulium atoms from optical dipole traps operating at 532 and 1064 nm, *Phys Rev A (Coll Park)* **107**, 023315 (2023).
- [47] V. V. Tsyganok et al., Bose-Einstein condensate as a diagnostic tool for an optical lattice formed by 1064-nm laser light, *Phys Rev A (Coll Park)* **108**, 013310 (2023).

- [48] E. T. Davletov, V. V. Tsyganok, V. A. Khlebnikov, D. A. Pershin, D. V. Shaykin, and A. V. Akimov, Machine learning for achieving Bose-Einstein condensation of thulium atoms, *Phys Rev A (Coll Park)* **102**, 011302 (2020).
- [49] A. Frisch, K. Aikawa, M. Mark, A. Rietzler, J. Schindler, E. Zupanič, R. Grimm, and F. Ferlaino, Narrow-line magneto-optical trap for erbium, *Phys Rev A (Coll Park)* **85**, 051401 (2012).
- [50] T. Maier, H. Kadau, M. Schmitt, A. Griesmaier, and T. Pfau, Narrow-line magneto-optical trap for dysprosium atoms, *Opt Lett* (2014).
- [51] T. H. Loftus, T. Ido, M. M. Boyd, A. D. Ludlow, and J. Ye, Narrow line cooling and momentum-space crystals, *Phys Rev A (Coll Park)* **70**, 063413 (2004).
- [52] B. Seo, P. Chen, Z. Chen, W. Yuan, M. Huang, S. Du, and G.-B. Jo, Efficient production of a narrow-line erbium magneto-optical trap with two-stage slowing, *Phys Rev A (Coll Park)* **102**, 013319 (2020).
- [53] E. Kalganova, O. Prudnikov, G. Vishnyakova, A. Golovizin, D. Tregubov, D. Sukachev, K. Khabarova, V. Sorokin, and N. Kolachevsky, Two-temperature momentum distribution in a thulium magneto-optical trap, *Phys Rev A (Coll Park)* **96**, 033418 (2017).
- [54] V. V. Tsyganok, D. A. Pershin, V. A. Khlebnikov, E. T. Davletov, and A. V. Akimov, Zeeman Spectroscopy of Ultracold Thulium Atoms, *Journal of Experimental and Theoretical Physics* **128**, (2019).
- [55] D. A. Kumpilov et al., Inspiration from machine learning on the example of optimization of the Bose-Einstein condensate of thulium atoms in a 1064-nm trap, *Phys Rev A (Coll Park)* **109**, (2024).